Article

Ultraviolet Radiation Environment of a Tropical Megacity in Transition: Mexico City 2000−2019

Adriana Ipiña,* Gamaliel López-Padilla, Armando Retama, Rubén D. Piacentini, and Sasha Madronich

Cite This: https://doi.org/10.1021/acs.est.0c08515

Read Online

ACCESS | Metrics & More | Article Recommendations | SI Supporting Information

ABSTRACT: Tropical regions experience naturally high levels of UV radiation, but urban pollution can reduce these levels substantially. We analyzed 20 years of measurements of the UV index (UVI) at several ground-level locations in the Mexico City Metropolitan Area and compared these data with the UVI values derived from the satellite observations of ozone and clouds (but not local pollution). The ground-based measurements were systematically lower than the satellite-based estimates by ca. 40% in 2000 and 25% in 2019. Calculations with a radiative transfer model using observed concentrations of air pollutants explained well the difference between satellite and ground-based UVI and showed specific contributions from aerosols, O_3, NO_2, and SO_2 in decreasing order of importance. Such large changes in UV radiation between 2000 and 2019 have important implications ranging from human health (skin cancer and cataract induction) to air pollution control (photochemical smog formation).

KEYWORDS: *UV radiation, urban pollution, Mexico City, air pollution, UV index*
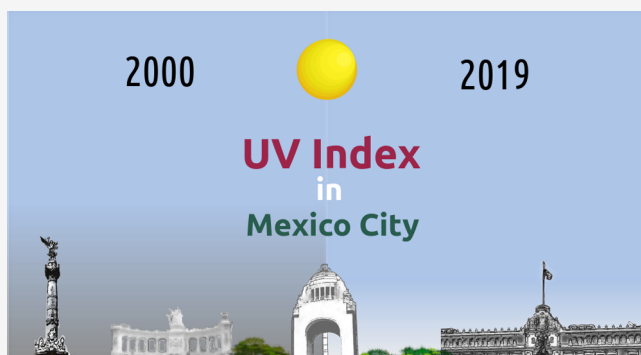
INTRODUCTION

Ultraviolet (UV) radiation is an important component of the urban environment, affecting human populations directly through UV exposure of skin and eyes[1−3] and less directly (but with great impact) by driving the formation of photochemical smog, including tropospheric ozone and other oxidants, as well as secondary aerosols containing nitrates, sulfates, and organics.[4−6] These pollutants, along with others of primary origin commonly found in urban atmospheres (e.g., black carbon and sulfur dioxide), can in turn scatter and/or absorb UV radiation, alter its vertical distribution, and thus modify the photochemical rate of their own formation. Such feedback complicates the calculation of both the UV radiation field (including at the surface) and the evolution of photochemical smog in the urban boundary layer (BL).

The question of how air pollution alters the urban UV radiation environment (and vice versa) is not new, but studies have relied mostly on numerical models[7−9] with relatively few available observations (e.g., McKenzie et al.,[10] Panicker et al.,[11] Palancar et al.,[12] and reviewed by Bais et al.[13]). Increases in UV have been estimated as a consequence of emission reductions over the last decades, for example, in China,[14−16] and have led to less-than-expected reductions in photochemical smog, in part due to stronger UV photochemistry.[17−19] Emission reductions have also occurred globally during the 2020 COVID-19 pandemic,[20,21] but ground-level ozone in some polluted areas has actually increased[22,23] due at least in part to

the increased UV radiation. Unfortunately, the observational database of relevant UV radiation remains rather sparse to evaluate such model-predicted feedbacks between chemistry and radiation.

The environment of Mexico City is of particular interest for several reasons: (1) nearly 23 million people inhabit the Mexico City Metropolitan Area (MCMA), and the UV radiation environment has direct implications for their health, both in terms of skin/eye UV exposure and *via* photochemical smog formation. (2) As a tropical megacity, it is to some extent representative of the situation of many others, with year-round intense midday UV irradiance, a shallower atmosphere due to the city's high elevation of 2240 m above sea level, and a transition toward newer and cleaner technologies, leading to gradual improvements in air quality. (3) The air quality within MCMA has undergone extensive scrutiny with a well-established monitoring network operating since 1986;[24] numerous intensive field campaigns to study the meteorology, emissions, and photochemistry of smog formation;[25−27] and numerical modeling incorporating the evolving knowl-

ACS Publications © XXXX American Chemical Society

A

edge.[28−31] This extensive body of knowledge provides the foundation for understanding our study.

In this work, we analyze 2 decades of continuous measurements of the UV index (UVI) at multiple locations within the MCMA, collected by the Secretariat of the Environment (Secretaría del Medio Ambiente, SEDEMA)[a] of the Mexico City government as part of an intensive monitoring network over the MCMA. The UVI is defined as

$$\text{UVI} = 40 \int_{250\,\text{nm}}^{400\,\text{nm}} E(\lambda, t) \cdot S_{\text{er}}(\lambda)\, \text{d}\lambda \tag{1}$$

where $E(\lambda, t)$ is the solar spectral irradiance in units of W·m^{-2}·nm^{-1} and $S_{\text{er}}(\lambda)$ is the erythemal sensitivity of human skin.[32,33] Multiplication by 40 was chosen historically to express the UVI in small integer numbers but is otherwise scientifically arbitrary.

The UVI is recognized by the World Health and Meteorological Organizations (WHO and WMO) as a standardized index of UV radiation[32] for global public information. An advantage of using the UVI as (one) measure of UV radiation is that it is being increasingly observed or calculated and disseminated, enabling more objective comparisons among seasons and locations. The UVI observations from Mexico City, considered here, are an important element of this global picture.

While the UVI at the surface cannot be translated directly into photolysis frequencies for various photolabile molecules, the spectral weighting of the UVI (ca. 300−320 nm) is approximately similar to that for the photolysis of ozone to singlet oxygen atoms. Other UV wavelengths are of course also important, for example, for the photolysis of nitrogen dioxide, and may be affected differently depending on the pollutant. With these considerations and a few other caveats, UVI trends examined here can also be used to infer accompanying trends in photolysis frequencies and influences on photochemical smog formation.

■ METHODS

Ground-Based Measurements. The MCMA is located at 19.4°N, 99.1°W, and 2240 m above sea level (m asl) surrounded by mountain ridges exceeding 5000 m asl, with complex topography and thermal inversions that inhibit winds and favor intense air pollution.[34−36] Air quality monitoring and surface meteorological measurements in the MCMA are conducted continuously by the Automated Atmospheric Monitoring Network (RAMA, by its Spanish acronym) of the Atmospheric Monitoring System (SIMAT, by its Spanish acronym) of the Mexico City government. Since the year 2000, UV radiometers (model 501-A, Solar Light Company Inc., Glenside, PA) detecting wavelengths between 280 and 400 nm have been measuring erythemally weighted solar radiation. Calibration of the UV sensors has been carried out annually by comparing against a factory-calibrated reference sensor. The output voltages from the network's sensors have been compared for at least 1 week against the UV readings from the reference sensor to derive new calibration factors, which typically differed from the old ones by 2% or less. Reference sensors were also calibrated by the manufacturer and updated periodically (between 3 and 5 years) to reduce systematic errors due to drifts in sensitivity. Long-term calibration drifts are minimized by these yearly re-calibrations. Although at the beginning only a few stations were in operation and varied, currently 11 stations are recording erythemal irradiances,

which are then multiplied by 40 (see eq 1) to give UV indices. Table 1 describes the location of the stations where the UVI

Table 1. SIMAT Stations and AERONET Site*, Environmental Descriptors, and Geographical Positions[a]

station	environment	lat (°N)	lon (°W)	El (m asl)
CHO	semi-urban	19.27	98.89	2253
CUT	ecological park	19.72	99.20	2263
FAC	urban	19.48	99.24	2299
HAN	urban	19.42	99.08	2235
LAA	urban	19.48	99.15	2255
MER	downtown	19.42	99.12	2245
MON	rural	19.46	98.90	2252
MPA	rural	19.18	98.99	2594
PED	residential	19.33	99.20	2326
SAG	urban	19.53	99.03	2241
SFE	residential	19.36	99.26	2599
TLA	urban	19.53	99.20	2311
UNAM*	University city	19.33	99.18	2294

[a]Abbreviations: Chalco (CHA), Cuautitlán (CUT), FES Acatlán (FAC), Hangares (HAN), Laboratorio de Análisis Ambiental (LAA), Merced (MER), Montecillo (MON), Milpa Alta (MPA), Pedregal (PED), San Agustín (SAG), Santa Fe (SFE), Tlalnepantla (TLA), and National Autonomous University of Mexico (UNAM*).

has been measured. Figure 1 shows how the radiometers of the SIMAT have been distributed over MCMA, prioritizing sites with higher population density. The near real-time data for each station are available on the SIMAT official website http://www.aire.cdmx.gob.mx/default.php. Daily maximum values (UVI$_{\text{max}}$) were extracted in each of the stations around solar noon from the time interval from 11:00 to 15:00 h CST (Central Standard Time). This database with 7305 continuous days of measurements during the period 2000−2019 was analyzed.

To explore the relationship between UVI and air pollutant levels, the hourly averages for ozone (O_3), carbon monoxide (CO), nitrogen dioxide (NO_2), sulfur dioxide (SO_2), and particle matter with diameter sizes ≤10 μm (PM_{10}) were downloaded from the SIMAT.[37] For purposes of assessing the influence on the UVI at solar noon, only values obtained between 11 and 15 h CST were considered for the trends analysis. Pollutant measurements are conducted by the SIMAT using regulatory-grade commercial instruments. The measurement principles include UV photometry (model 400E, Teledyne-API) for O_3, chemiluminescence (model 200E, Teledyne-API) for NO_2, UV fluorescence (model 100E, Teledyne API) for SO_2, and infrared absorption (model 300E, Teledyne API) for CO. The PM_{10} continuous mass concentration was measured with Tapered Element Oscillating Microbalance (TEOM 1400AB or TEOM 1405 DF, Thermo Scientific) monitors. Gaseous pollutant levels are reported in ppb concentration units for O_3, SO_2, and NO_2 and in ppm for CO. The particulate matter mass concentration is reported in μg m^{-3} at local temperature and pressure.

The aerosol optical depth at 340 nm was obtained from the Institute of Geophysics of the National Autonomous University of Mexico (UNAM). Measurements were conducted with a CIMEL sun photometer model CE-318, which is an automatic sun-sky-scanning spectral radiometer of the Aerosol Robotic Network (AERONET[38]). The data Product Level 2.0 and 1.5 (only in 2019) were selected, and the annual
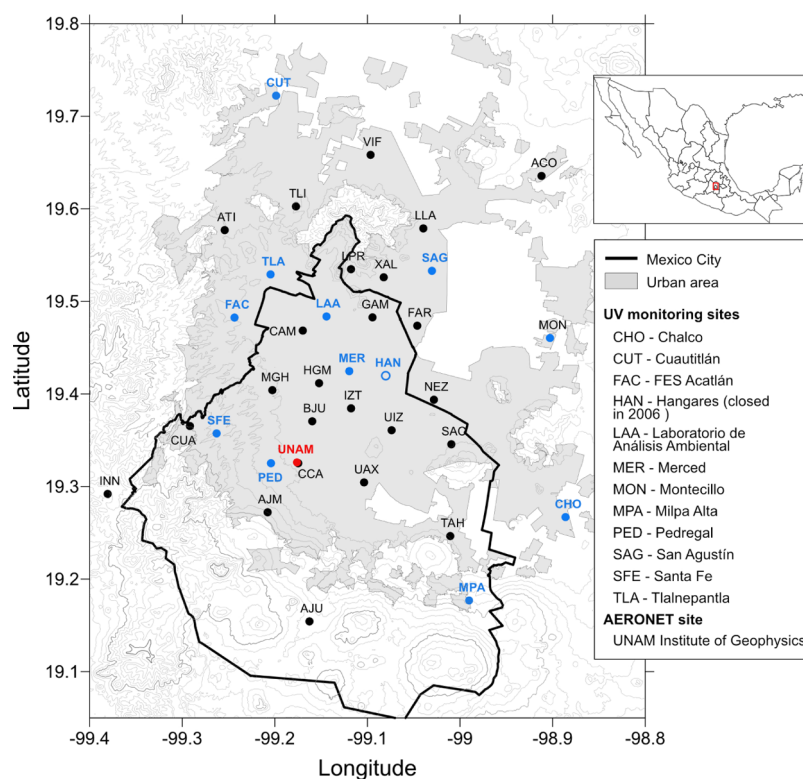
Figure 1. Map with the location of the SIMAT continuous monitoring stations over MCMA. Sites denoted by the blue solid dots correspond to SIMAT stations with UV measurements, while the black dots indicate SIMAT stations without UV measurements, the site indicated by an open blue dot represents a discontinued site, and the red dot shows the location of the AERONET site. The location of Mexico City and the acronyms of the UV and AERONET site are shown at the upper and lower frames at the right, respectively.

averages of AOD_{340} were calculated for the period 2000−2019, except for the year 2011 which contained large data gaps and was therefore not used. A previous study of the AOD behavior from 2000 to 2014 demonstrated that data gaps did not significantly change the trends calculated for this time period.[39] Only 8% of the data between the years 2014 and 2019 were missing. The largest data gap occurred in 2018 when the instrument was returned for calibration.

Satellite Data. The UVI data derived from satellite-based measurements were used for comparison with the ground-based measurements. These data were provided by the Ozone Monitoring Instrument (OMI) on board of the AURA-NASA satellite.[40] OMI is operated collaboratively by the Netherlands Agency for Aerospace Programmes (NIVR), the Finnish Meteorological Institute (FMI), and NASA. OMI performs observations over a geographical area of 13×24 km^2 at nadir. For the coordinates (19.33°N, 99.18°W) and elevation (2268 m asl) of Mexico City, the satellite overpass time is between 19:00 and 21:00 h UTC (13:00−15:00 h CST). The OMI instrument measures reflected and backscattered radiances of the atmosphere−surface system at several UV wavelengths.[41] The ozone column is estimated by differential absorption of several adjacent wavelengths in the O_3 Huggins band[42] and is used in a radiative transfer model to estimate clear-sky UVI at the surface. The clouds are estimated from the observed reflectivity at a wavelength not affected by O_3 absorption (360 nm) and the clear-sky UVI is adjusted for their presence.[43] A correction for absorbing aerosols is made using a global aerosol climatology.[44] The UVI used for Mexico City corresponds to values at local noon time and clear sky from the OMUVB Level 2 OVP data product, version 1.3 and collection 3.

TUV Model. Calculations of the UVI were also made with the Tropospheric Ultraviolet Visible (TUV v5.3) model.[45] The model atmosphere is represented by 80 vertical layers, each 1 km thick, starting at the 2.24 km asl elevation of MCMA, and for which the first 3 km constitutes the atmospheric BL.[46] The ozone profile above the BL is from the US Standard Atmosphere but rescaled to a value of 259.6 DU. The total ozone columns including the BL contributions (of 13.7 DU in the year 2000 and 9.8 DU in 2019, see below) were 273.1 DU in 2000 and 269.2 DU in 2019, respectively. The climatological O_3 column for this latitude and season is about 270 DU (plus or minus ca. 5 DU), which is in good agreement with the values used here.

Pollutants within the BL (including O_3) are assumed to be well mixed in agreement with observations from the MILAGRO field campaign that showed the disappearance of vertical gradients in the profiles of gases[47,48] and aerosols[49,50] by late morning. The UV-absorbing gases considered here are O_3, NO_2, and SO_2, specified in ppb.

BL aerosols are modeled by prescribing the AOD at 340 nm (from AERONET observations), scaled to other wavelengths inversely with wavelength (Angstrom coefficient = 1.0), asymmetry factor of 0.7, and a single scattering albedo of 0.85 at UV wavelengths, following the determinations made in Mexico City by Corr et al.[51] and Palancar et al.[12]

Above the atmospheric BL, the model atmosphere was specified to be free of aerosols, NO_2, or SO_2. In one sensitivity study, a total AOD of 0.7 was redistributed placing 0.2 in the free troposphere (decreasing vertically with an exponential scale height of 4 km and 0.5 remaining in the BL). The calculated UVI differed by less than 1%. Thus, as long as the
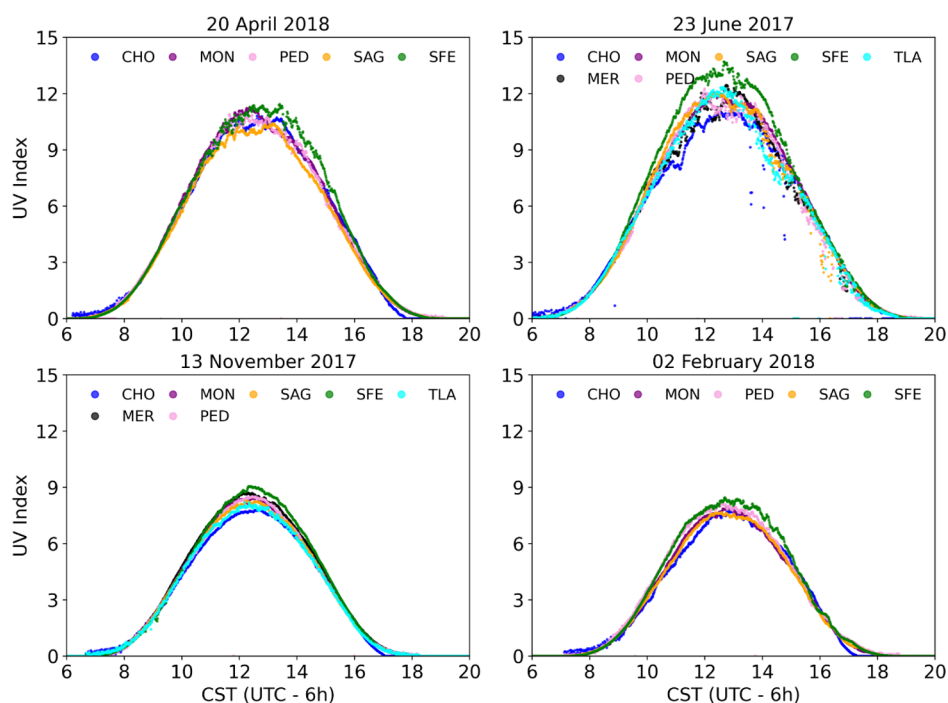
Figure 2. UVI measurements at 1 min resolution from several SIMAT stations within the MCMA under mostly cloudless conditions for representative days of the year.

total AOD is known, the knowledge of the exact vertical aerosol profile is not critical for ground-level UVI, though it would obviously affect the vertical structure of photolysis frequencies.

Radiative transfer calculations were carried out with the pseudo-spherical 4-stream option at 1 nm steps between 280 and 420 nm.

RESULTS AND DISCUSSION

Figure 2 shows the diurnal variation of the UVI for typical cloud-free days for different seasons and several locations (CHO, MER, MON, PED, SAG, SFE, and TLA). The selection of cloud-free days was aided by comparison of the measurements with the TUV model predictions for clear skies, with prolonged deviations and fluctuations usually indicative of cloudy conditions. However, during the rainy period (from June to October), at least a brief episode of clouds is seen at the CHO station around noon on 23 June 2017. The peak values range from 8 during autumn/winter to above 12 in spring/summer in correspondence to the respective December and June solstices. Although the stations are all within a 25 km radius, substantial differences among them are notable. The survey of the locations revealed that shadowing from nearby structures is not an issue. The good agreement in the morning, followed by more divergence in the afternoon, is consistent with the development of photochemical pollution hotspots during the day. Previous studies (e.g., Castro et al.[52] and Palancar et al.[12]) have shown that surface UV radiation in Mexico City is attenuated significantly by aerosols. The measurements shown in Figure 2 are consistent with this increasing pollution during the course of the day, with highest aerosol loading (and highest variability) attained in the afternoon. Further support for the role of pollution in suppressing the UVI comes from the observation made at the Santa Fe (SFE) site, which in Figure 2 are shown to be

systematically higher, for example, by over 10% in autumn afternoons, compared to the other stations. The SFE station is displaced to the west from the majority of the other stations and remains in the outskirts. This site is also approximately 300 m higher than Mexico City downtown, so that the cleaner atmosphere at SFE is a result of the station's location farther away from pollution sources, both horizontally and vertically.[53] It is indeed expected to have higher values of the UVI in agreement with the observations.

The daily maximum UVI values of each station, UVI$_{max}$, are summarized in Figure 3 for the entire period 2000−2019. These values are seen to range from 1 to 16 with a majority (61%) of the days experiencing UVI$_{max}$ values between 6 and 10, and remarkably few, less than 1%, in the 13−16 range. The
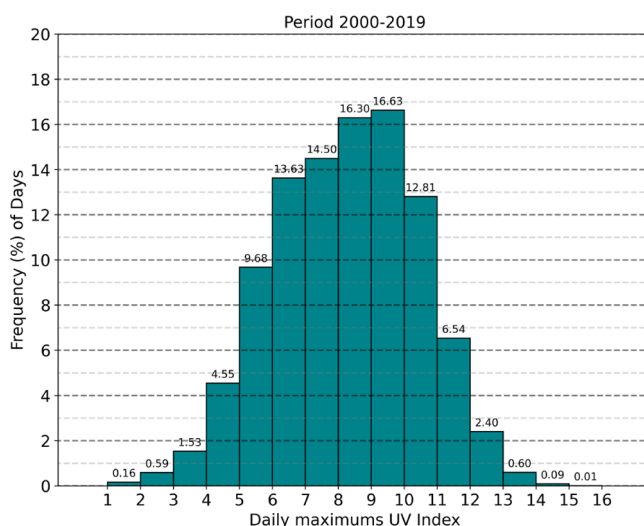

Figure 3. Frequency distribution of daily maximums UVI values in Mexico City for the period 2000−2019.
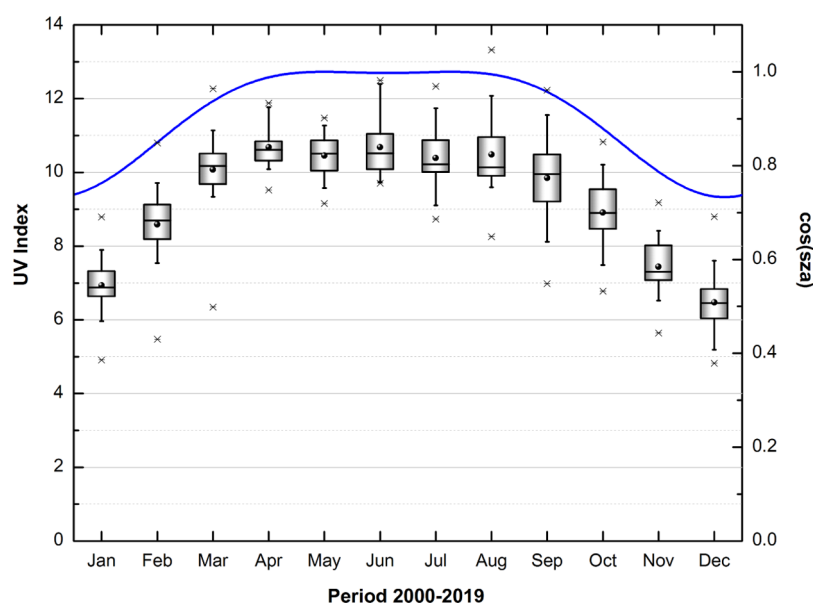
Figure 4. Monthly averages of the maximum UVI values (black dot) in MCMA for the period 2000−2019: median (central bold line), interquartile range (box edges), 10 and 90% percentiles (whiskers), the minimum and maximum values (asterisk), and the cosine of the solar zenith angle at solar noon (blue curve).

lowest values are likely due to winter days with heavy cloud cover and low sun angles, and UV attenuation by pollutants could also be amplified under such conditions due to longer photon path lengths at low sun and within clouds. The extreme sparsity of high UVI values remains surprising and may be an indication of the rarity of extremely unpolluted days within the city.

Similar patterns are found when considering the monthly average of the UVI_{max} values as shown in Figure 4. The long-term averages present a seasonal variation (as shown in Figure 2) that follows approximately the cosine of the noontime solar zenith angle. Notably, the values rarely if ever exceed 12 (as shown in Figure 3). The lowest average UVI (near 7) occurs in winter, while from March to August, the values seem to be flattened in the range 10−11. The rather low monthly UVI values could be a consequence of the presence of clouds in the rainy season. However, urban aerosol pollution sources, biomass burning for agriculture, and wood cooking also contribute to poor air quality between March−May.[54] Using the maximum UVI_{max} from all of stations every day (one daily point), the monthly averages ($\overline{UVI}_m$) were calculated along the period 2000−2019 (except for June 2003 due to lack of measurements). Long-term trends in $\overline{UVI}_m$ are shown in Figure 5. A clear upward trend is seen with a slope for the linear fit of 0.9%/year or +1.5 UVI units over the 2 decades.

The UVI computed from OMI satellite-based observations over the period 2005−2019 is shown in Figure 6. The satellite-derived UVIs vary from 8 in winter to 16 in summer, these values being substantially higher than the ground-based observations (ca. 7 for winter and 11 for summer, see Figure 4). The maximum values are reached in June and July of each year for both data sets. We hypothesize that this large difference between satellite-based estimation and ground-based observation of the UVI is due to the intense air pollution of Mexico City. A rather similar behavior was detected in the city of Santiago, Chile.[55] Although the OMI data are corrected for climatological aerosol absorption,[44] this correction likely
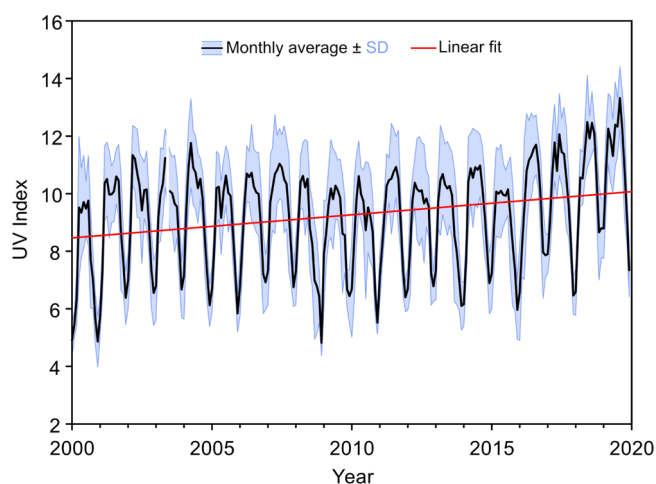
underestimates the absorption within the polluted Mexico City BL.

Figure 7 shows the deviation of the OMI-derived UVI from the ground-based monthly averages. The mean deviation was 35% in the period 2005−2019. Comparable UV reductions, of 30−40% due to aerosols, were reported by Panicker et al.[11] over Pune, India, from April 2004 to March 2005, with sensitivity coefficients (i.e., change in UVI per unit change in AOD).

Comparisons of OMI with ground-based UV measurements have been reviewed recently by Zhang et al.[56] and Vitt et al.[57] OMI-derived UV generally overestimates ground-level measurements by 1−10% in relatively clean conditions (e.g., rural U.S.) by 10−30% in Southern Europe and by 40% or more in Santiago, Chile[55] and Thailand.[58] The overestimations appear related in large part to incomplete accounting of UV absorption by BL aerosol, although other factors such as the correction to solar noon may also introduce some bias.[56] Over
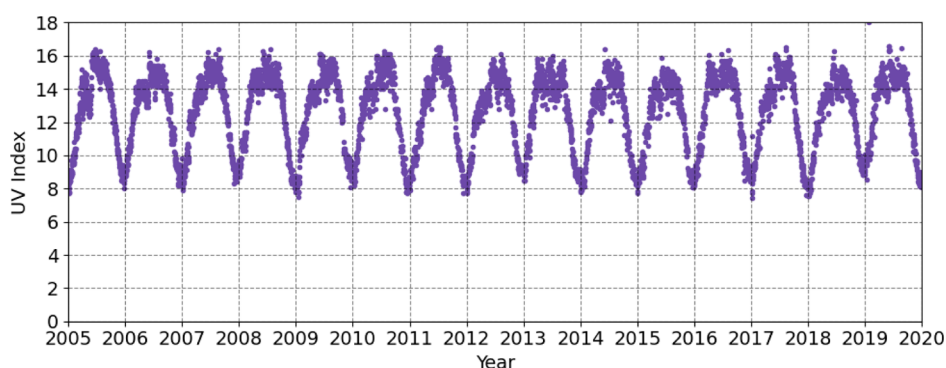

Figure 5. Monthly average UVI (black line), the standard deviation (blue fill area), and linear fit (red line).

Figure 6. UVI at solar noon for clear sky recorded by OMI-Aura/NIVR-FMI-NASA, from 2005 to 2019.
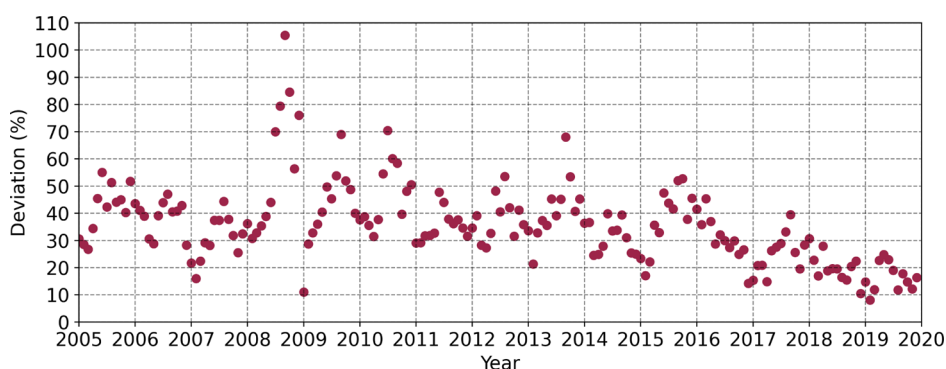

Figure 7. Deviation (%) of satellite-derived UVI from the ground-based monthly means UVI for the period 2005−2019.

Europe, ground-based UVI observations for several decades are systematically lower than those estimated from satellites even after consideration of climatological aerosol distributions, showing the importance of local pollution not resolved from space.[57] However, the difference between satellite-derived and ground-based UVI was less than 1.0 UVI units in over 90% of the cases in contrast to the difference of 3−5 units found here for Mexico City.

Effect of Pollutants on UV Radiation in Mexico City. Trends and averages in aerosol optical depth AOD_{340} and criteria pollutants PM_{10}, CO, NO_2, O_3, and SO_2 observed at the SIMAT stations over 2000−2019 are shown in Figure 8 and summarized in Table 2 together with the UVI_{max}. Similar trends in pollutants have been noted before[59−61] and reflect the long-term success of emission reduction policies and programs.

The observed changes in the concentrations of these air pollutants have significant implications for surface UV radiation, as can be demonstrated with the TUV radiative transfer model. Table 3 summarizes the UVI values for the June−July time period, estimated by the three methods: OMI satellite-derived UVI, SIMAT ground-based observations, and TUV modeling using air pollution estimates. Two groups of values can be readily identified: (1) SIMAT daily record values, OMI with or without BL aerosols, and TUV for very clean conditions, all with UVI values around 15−16 and (2) the average of daily maxima of SIMAT observations and TUV UVI results using MCMA pollutants as the input. Note that SIMAT and TUV value are in good agreement for both 2000−2001 and 2018−2019 and are considerably lower than for group (1). Compared to the OMI estimate that included the climatological absorbing aerosol correction (16.6), the observed SIMAT values were lower by 40% in 2000 and by

25% in 2019. Similarly, the TUV values were 35% lower in 2000 and 22% lower in 2019 relative to the TUV values of 15.6 for a pristine atmosphere.

The agreement between SIMAT observations and TUV model estimates is excellent but also probably a bit fortuitous. Clouds on an average reduce the irradiance impingent on the surface, but scattering from them can also cause transient enhancements (these are only possible if the disk of the Sun is visible) that could be recorded as daily maxima—with cancellation between these cloud effects resulting in improved agreement with the cloud-free model. We cannot exclude that some of the observed trend in UVI is due to changes in cloud cover. However, the modeled UVI reductions due to pollutants, shown in Table 3, are in such good agreement with the observed UVI reductions such that a compelling case can be made for a dominant role of air pollutants in the long-term UVI trends.

Table 4 shows the contribution to UVI reductions from individual pollutants computed with the TUV model for conditions similar to those in Table 3 (21 June solar noon). If the pollutant levels of the year 2000 are added one at the time to a pollution-free atmosphere (see middle column of Table 4), aerosols account for more than half of the total UVI reduction, with the gases O_3, NO_2, and SO_2, contributing in order of importance to the remainder. It should be noted that the sum of these individual contributions (−6.8) differs from the value obtained if these pollutants are applied simultaneously rather than one at the time (−5.9, from Table 3). This non-additivity results mainly from (1) saturation of overlapping absorption spectra, especially for O_3 and SO_2 at the shortest wavelengths, and (2) interactions between absorption and scattering, for example, aerosols, causing a change in
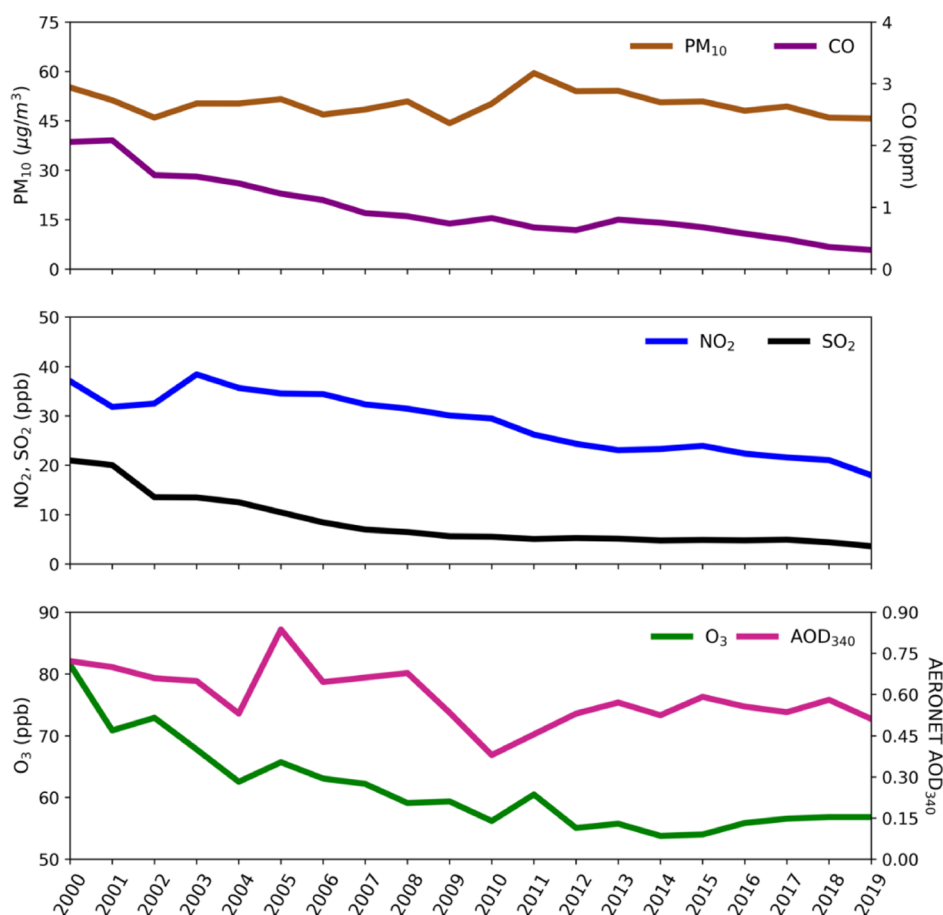
Figure 8. Air quality trends in MCMA for the period 2000−2019. Annual averages obtained between 11 and 15 h CST every day: PM_{10} (brown curve), CO (purple curve), NO_2 (blue curve), SO_2 (black curve), O_3 (green curve), and AOD_{340} (magenta curve).

Table 2. Trends of UVI and Criteria Pollutants over 2000−2019[a]

variable	absolute change/year	Avg$_{2000-2019}$	Δ (%/year)
UVI	0.08	9.2	0.9
PM_{10}	−0.10	50.2	−0.2
CO	−0.08	1.0	−8.2
NO_2	−0.96	28.6	−3.4
O_3	−1.05	61.3	−1.7
AOD_{340}	−0.01	0.6	−1.6
SO_2	−0.76	8.4	−9.1

[a]Units: $\mu g/m^3$ for PM_{10}, ppm for CO, ppb for SO_2, NO_2, and O_3.

Table 3. Comparison of June−July UVI Maxima Measured Directly (SIMAT), Inferred from Satellite-Based Observations (OMI), and Modeled for Different Pollution Levels (TUV Calculation for 21 June at Solar Noon)

June−July	UVI
SIMAT average maxima 2000−2001	9.9 ± 1.2
SIMAT average maxima 2018−2019	12.3 ± 1.3
SIMAT maximum value reached in period 2000−2019	15.0
OMI maximum value reached in period 2005−2019	16.6
TUV "Zero" Pollution	
AOD 0, O_3 0 ppb, NO_2 0 ppb, SO_2 0 ppb	16.1
TUV Pristine Atmosphere	
AOD 0.05, O_3 10 ppb, NO_2 0 ppb, SO_2 0 ppb	15.6
TUV 2019	
AOD 0.5, O_3 50 ppb, NO_2 20 ppb, SO_2 1 ppb	12.1
TUV 2000	
AOD 0.7, O_3 70 ppb, NO_2 40 ppb, SO_2 20 ppb	10.2

photon pathlengths through absorbing gases; both effects are treated in the TUV model.

The right column of Table 4 shows the contribution of the individual pollutants to the UVI increase experienced over the years 2000−2019. For this calculation, the pollutants were decreased individually to their 2019 level while the others were held at the 2000 values. Aerosol reductions were the largest single factor responsible for the UV increase, but more than half of the increase was due to reductions of the gases, of which the near-complete elimination of SO_2 was most important. The total increase computed from the sum (1.8) is in good agreement with the 2000−2019 increase in which all pollutants were changed simultaneously (1.9, from Table 3), as smaller changes in UVI mitigate non-linearities.

UV reductions by air pollutants are expected to be most severe near the surface, while chemical reactions leading to photochemical smog occur throughout the vertical extent of the BL. Figure 9 shows the vertical profiles of photolysis coefficients (the reciprocals of photolytic lifetimes) computed with the TUV model for two key reactions: photolysis of O_3 to yield excited oxygen atoms $O(^1D)$ and photolysis of NO_2. In the absence of optically active pollutants, these coefficients would be nearly independent of altitude in the BL. However, the presence of pollutants leads to a strong decrease toward the

Table 4. Contribution of Different Pollutants to UVI Changes in Mexico City Calculated with the TUV Model for 21 June at Solar Noon[a]

pollutant	ΔUVI, 2000—zero pollution[a]	ΔUVI, 2000–2019[b]
AOD	−3.7	0.8
O_3	−1.4	0.3
NO_2	−0.9	0.3
SO_2	−0.8	0.4
total	**−6.8**	**1.8**

[a]Pollutants from year 2000 added to a clean atmosphere, one at the time. [b]Pollutants lowered from 2000 to 2019 levels, one at the time.

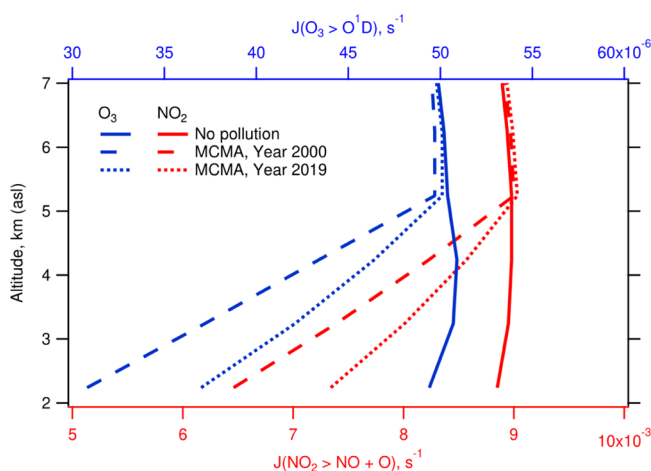**Figure 9.** Vertical profiles of the photolysis coefficients for the reaction $O_3 + h\nu \rightarrow O(^1D) + O_2$ (top axis, blue) and $NO_2 + h\nu \rightarrow O + NO$ (bottom axis, red) for zero pollution (solid) and Mexico City in the years 2000 (dashed) and 2019 (dotted). TUV calculation for 21 June at solar noon.

surface, with notably more severe reductions in 2000 compared to 2019. While the specific values shown in the figure are only illustrative for typical conditions, routine daily air quality modeling should carefully account for the long-term variations in these photolysis coefficients.

An issue that is beginning to gain relevance in radiative balance models is the influence of a group of organic compounds known as "brown carbon" that are capable of strongly absorbing in the UV region.[62] Some of these compounds are related to emissions from local and regional wildfires.[63] Mexico City is frequently exposed to regional fire smoke transport during the dry part of the year (November to May),[64] which sporadically modify the optical properties of the aerosols.[65] This could partly explain the relatively minor reductions in PM_{10} (see Figure 8) compared to the larger reductions of CO, NO_2, and O_3 that are more directly related to urban activities, as well as some of the seasonal asymmetry seen in Figure 3.

The UVI is specific to wavelengths mainly in the 300–320 nm range, and so the question remains whether these results can be applied at longer UV wavelengths, for example, those important for NO_2 photolysis (<420 nm). Absorption by SO_2 and O_3 vanishes for wavelengths larger than about 330 nm, while NO_2 photolysis is mostly driven by UV-A radiation, and typical aerosols' optical depth decreases with the wavelength. These changes can easily be modeled, but unfortunately, far fewer measurements of these longer wavelengths are available in Mexico City or elsewhere.

Two decades of observations in Mexico City demonstrate unequivocally that air pollution reduces UV radiation at the ground. The ground-based observations are well below the values derived from satellite-based observations. Although ideally both data sets should match, the limited ability of satellites to detect BL absorbers means that they cannot reveal long-term UV trends due to substantial air quality improvements that are evident in the ground-based UVI data. When typical values of pollutant aerosols, tropospheric ozone, NO_2 and SO_2, are included in a model (e.g., TUV), the differences between satellite-derived and ground-based measured values are explained and can be attributed quantitatively to individual observed pollutants. Long-term improvements in air quality over the last 2 decades were accompanied by statistically significant increases in the observed UVI in agreement with the model-predicted changes.

The reductions in surface UV radiation with respect to an ideally clear atmosphere—by nearly 40% in 2000 and still 20% in 2019—are large, both within the context of human UV exposure and air quality mitigation. In urban areas where ozone production scales proportionally with UV levels and with volatile organic compound (VOC) emissions (the VOC-limited regime), a 10% increase in BL average photolysis rates indicates that VOC emissions will need to be reduced by 10% to meet the same goals, or else successful reductions in aerosols would lead to unwanted UV-driven increases in O_3. Such UV changes must be considered carefully in air quality mitigation strategies. For human exposure, a 20% increase in UV irradiances over 2 decades should be seen as a non-negligible public health issue requiring some reassessment of preventive behaviors to minimize the risk of skin cancer, cataract, and other UV-related health effects. The efforts that Mexico City has made to improve the air quality have reduced the levels of most air pollutants. Nevertheless, they caused an increase in UV radiation that reaches the surface.

Finally, based on our results, the solar radiation monitoring network might be improved by adding observation sites far enough away to lessen the influence of the urban plume (e.g., Amecameca; latitude: 19.13°N, longitude: 99.76°W, and elevation: 2420 m asl) and the adding sensors to existing monitoring sites at higher elevations (Ajusco, AJU, 2953 m asl or Instituto de Investigaciones Nucleares, INN, 3082 m asl). These sites would provide valuable observations to assess quantitatively the effects of urban pollution on solar radiation levels.

■ ASSOCIATED CONTENT

Ⓢ Supporting Information

The Supporting Information is available free of charge at https://pubs.acs.org/doi/10.1021/acs.est.0c08515.

(PDF)

■ AUTHOR INFORMATION

Corresponding Author

Adriana Ipiña − *Instituto de Física Rosario (CONICET-UNR), 2000 Rosario, Argentina; Centro de Ciencias de la Atmósfera, Universidad Nacional Autónoma de México, 04510 Mexico City, Mexico;* ⓞ orcid.org/0000-0001-7764-4830; Email: ipina@ifir-conicet.gov.ar

Authors

Gamaliel López-Padilla − *Facultad de Ciencias Físico Matemáticas, Universidad Autónoma de Nuevo León, 66451 San Nicolás de los Garza, Mexico*

Armando Retama − *Independent Researcher, 11800 Mexico City, Mexico*

Rubén D. Piacentini − *Instituto de Física Rosario (CONICET-UNR), 2000 Rosario, Argentina*

Sasha Madronich − *National Center for Atmospheric Research, Boulder 80307 Colorado, United States;* orcid.org/0000-0003-0983-1313

Complete contact information is available at:
https://pubs.acs.org/10.1021/acs.est.0c08515

Notes

The authors declare no competing financial interest.

■ ADDITIONAL NOTE

[a]https://www.sedema.cdmx.gob.mx/.

■ REFERENCES

(1) Taylor, H. R.; West, S. K.; Rosenthal, F. S.; Muñoz, B.; Newland, H. S.; Abbey, H.; Emmett, E. A. Effect of Ultraviolet Radiation on Cataract Formation. *N. Engl. J. Med.* **1988**, *319*, 1429−1433.

(2) Varotsos, C.; Feretis, E. Health effects on human eye resulting from the increased ambient solar ultraviolet radiation. *Toxicol. Environ. Chem.* **1997**, *61*, 43−68.

(3) Lucas, R. M.; Yazar, S.; Young, A. R.; Norval, M.; de Gruijl, F. R.; Rhodes, L. E.; Sinclair, C. A.; Neale, R. E.; Neale, R. E. Human health in relation to exposure to solar ultraviolet radiation under changing stratospheric ozone and climate. *Photochem. Photobiol. Sci.* **2019**, *18*, 641−680.

(4) Leighton, P. A. *Photochemistry of Air Pollution*; Elsevier, 1961; pp v−vi.

(5) Seinfeld, J. H.; Pandis, S. N.; Noone, K. Atmospheric Chemistry and Physics: From Air Pollution to Climate Change. *Phys. Today* **1998**, *51*, 88−90.

(6) Finlayson-Pitts, B. J.; Pitts, J. N. *Chemistry of the Upper and Lower Atmosphere*; Academic Press, 2000; pp xvii−xviii.

(7) Liu, S. C.; McKeen, S. A.; Madronich, S. Effect of anthropogenic aerosols on biologically active ultraviolet radiation. *Geophys. Res. Lett.* **1991**, *18*, 2265−2268.

(8) Sabziparvar, A. A.; de F Forster, P. M.; Shine, K. P. Changes in ultraviolet radiation due to stratospheric and tropospheric ozone changes since preindustrial times. *J. Geophys. Res.: Atmos.* **1998**, *103*, 26107−26113.

(9) Madronich, S.; Wagner, M.; Groth, P. Influence of Tropospheric Ozone Control on Exposure to Ultraviolet Radiation at the Surface. *Environ. Sci. Technol.* **2011**, *45*, 6919−6923.

(10) McKenzie, R. L.; Weinreis, C.; Johnston, P. V.; Liley, B.; Shiona, H.; Kotkamp, M.; Smale, D.; Takegawa, N.; Kondo, Y. Effects of urban pollution on UV spectral irradiances. *Atmos. Chem. Phys.* **2008**, *8*, 5683−5697.

(11) Panicker, A. S.; Pandithurai, G.; Takamura, T.; Pinker, R. T. Aerosol effects in the UV-B spectral region over Pune, an urban site in India. *Geophys. Res. Lett.* **2009**, *36*, L10802.

(12) Palancar, G. G.; Lefer, B. L.; Hall, S. R.; Shaw, W. J.; Corr, C. A.; Herndon, S. C.; Slusser, J. R.; Madronich, S. Effect of aerosols and NO_2 concentration on ultraviolet actinic flux near Mexico City during MILAGRO: measurements and model calculations. *Atmos. Chem. Phys.* **2013**, *13*, 1011−1022.

(13) Bais, A. F.; McKenzie, R. L.; Bernhard, G.; Aucamp, P. J.; Ilyas, M.; Madronich, S.; Tourpali, K. Ozone depletion and climate change: impacts on UV radiation. *Photochem. Photobiol. Sci.* **2015**, *14*, 19−52.

(14) Hollaway, M.; Wild, O.; Yang, T.; Sun, Y.; Xu, W.; Xie, C.; Whalley, L.; Slater, E.; Heard, D.; Liu, D. Photochemical impacts of haze pollution in an urban environment. *Atmos. Chem. Phys.* **2019**, *19*, 9699−9714.

(15) Li, K.; Jacob, D. J.; Liao, H.; Shen, L.; Zhang, Q.; Bates, K. H. Anthropogenic drivers of 2013-2017 trends in summer surface ozone in China. *Proc. Natl. Acad. Sci. U.S.A.* **2018**, *116*, 422−427.

(16) Wang, Y.; Gao, W.; Wang, S.; Song, T.; Gong, Z.; Ji, D.; Wang, L.; Liu, Z.; Tang, G.; Huo, Y.; Tian, S.; Li, J.; Li, M.; Yang, Y.; Chu, B.; Petäjä, T.; Kerminen, V.-M.; He, H.; Hao, J.; Kulmala, M.; Wang, Y.; Zhang, Y. *Contrasting Trends of PM2.5 and Surface-Ozone Concentrations in China from 2013 to 2017*; Oxford University Press (OUP), 2020; Vol. 7, pp 1331−1339.

(17) Wang, W.; Li, X.; Shao, M.; Hu, M.; Zeng, L.; Wu, Y.; Tan, T. The impact of aerosols on photolysis frequencies and ozone production in Beijing during the 4-year period 2012−2015. *Atmos. Chem. Phys.* **2019**, *19*, 9413−9429.

(18) Gao, J.; Li, Y.; Zhu, B.; Hu, B.; Wang, L.; Bao, F. What have we missed when studying the impact of aerosols on surface ozone via changing photolysis rates? *Atmos. Chem. Phys.* **2020**, *20*, 10831−10844.

(19) Ma, X.; Huang, J.; Zhao, T.; Liu, C.; Zhao, K.; Xing, J.; Xiao, W. Rapid increase in summer surface ozone over the North China Plain during 2013−2019: a side effect of particulate matters reduction control? *Atmos. Chem. Phys.* **2021**, *21*, 1−16.

(20) Bauwens, M.; Compernolle, S.; Stavrakou, T.; Müller, J.-F.; Gent, J.; Eskes, H.; Levelt, P. F.; A, R.; Veefkind, J. P.; Vlietinck, J.; Yu, H.; Zehner, C. Impact of coronavirus outbreak on NO_2 pollution assessed using TROPOMI and OMI observations. *Geophys. Res. Lett.* **2020**, *47*, No. e2020GL087978.

(21) Venter, Z. S.; Aunan, K.; Chowdhury, S.; Lelieveld, J. COVID-19 lockdowns cause global air pollution declines. *Proc. Natl. Acad. Sci. U.S.A.* **2020**, *117*, 18984−18990.

(22) Shi, X.; Brasseur, G. P. The Response in Air Quality to the Reduction of Chinese Economic Activities During the COVID-19 Outbreak. *Geophys. Res. Lett.* **2020**, *47*, No. e2020GL088070.

(23) Le, T.; Wang, Y.; Liu, L.; Yang, J.; Yung, Y. L.; Li, G.; Seinfeld, J. H. Unexpected air pollution with marked emission reductions during the COVID-19 outbreak in China. *Science* **2020**, *369*, 702−706.

(24) Secretaría del Medio Ambiente. Gobierno de la Ciudad de México, México, Red Automática de Monitoreo Atmosférico (RAMA). http://www.aire.cdmx.gob.mx/descargas/datos/excel/RAMAxls.pdf (accessed on 2021-06-16).

(25) Doran, J. C.; Bian, X.; de Wekker, S. F. J.; Edgerton, S.; Fast, J. D.; Hubbe, J. M.; Shaw, W. J.; Whiteman, C. D.; Abbott, S.; Fernandez, C.; Leach, J.; Mulhearn, M.; Russell, C.; Templeman, B.; Wolfe, D.; Archuleta, J.; Elliott, S.; Fernandez, A.; Langley, D.; Lee, J. T.; Porch, W.; Tellier, L.; Chow, J.; Watson, J. G.; Coulter, R. L.; Martin, T. J.; Shannon, J. D.; White, R.; Martinez, D.; Martinez, J. L.; Mora, V.; Sosa, G.; Mercado, G.; Pena, J. L.; Salas, R.; Petty, R. The IMADA-AVER Boundary Layer Experiment in the Mexico City Area. *Bull. Am. Meteorol. Soc.* **1998**, *79*, 2497−2508.

(26) Molina, L. T.; Kolb, C. E.; de Foy, B.; Lamb, B. K.; Brune, W. H.; Jimenez, J. L.; Ramos-Villegas, R.; Sarmiento, J.; Paramo-Figueroa, V. H.; Cardenas, B.; Gutierrez-Avedoy, V.; Molina, M. J. Air quality in North America's most populous city - overview of the MCMA-2003 campaign. *Atmos. Chem. Phys.* **2007**, *7*, 2447−2473.

(27) Molina, L. T.; Madronich, S.; Gaffney, J. S.; Apel, E.; de Foy, B.; Fast, J.; Ferrare, R.; Herndon, S.; Jimenez, J. L.; Lamb, B.; Osornio-Vargas, A. R.; Russell, P.; Schauer, J. J.; Stevens, P. S.; Volkamer, R.; Zavala, M. An overview of the MILAGRO 2006 Campaign: Mexico City emissions and their transport and transformation. *Atmos. Chem. Phys.* **2010**, *10*, 8697−8760.

(28) Jazcilevich, A. D.; García, A. R.; Caetano, E. Locally induced surface air confluence by complex terrain and its effects on air pollution in the valley of Mexico. *Atmos. Environ.* **2005**, *39*, 5481−5489.

(29) Tie, X.; Madronich, S.; Li, G.; Ying, Z.; Zhang, R.; Garcia, A. R.; Lee-Taylor, J.; Liu, Y. Characterizations of chemical oxidants in Mexico City: A regional chemical dynamical model (WRF-Chem) study. *Atmos. Environ.* **2007**, *41*, 1989−2008.

(30) Zhang, Y.; Dubey, M. K.; Olsen, S. C.; Zheng, J.; Zhang, R. Comparisons of WRF/Chem simulations in Mexico City with ground-based RAMA measurements during the 2006-MILAGRO. *Atmos. Chem. Phys.* **2009**, *9*, 3777−3798.

(31) Zavala, M.; Brune, W. H.; Velasco, E.; Retama, A.; Cruz-Alavez, L. A.; Molina, L. T. Changes in ozone production and VOC reactivity in the atmosphere of the Mexico City Metropolitan Area. *Atmos. Environ.* **2020**, *238*, 117747.

(32) WHOWMO; UNEP; ICNIRP. *Global Solar UV Index : A Practical Guide*, 2002; pp A joint recommendation of the World Health Organization, World Meteorological Organization, United Nations Environment Programme, and the International Commission on Non−Ionizing Radiation Protection.

(33) Webb, A. R.; Slaper, H.; Koepke, P.; Schmalwieser, A. W. Know Your Standard: Clarifying the CIE Erythema Action Spectrum. *Photochem. Photobiol.* **2011**, *87*, 483−486.

(34) Whiteman, C. D.; Zhong, S.; Bian, X.; Fast, J. D.; Doran, J. C. Boundary layer evolution and regional-scale diurnal circulations over the and Mexican plateau. *J. Geophys. Res.: Atmos.* **2000**, *105*, 10081−10102.

(35) Fast, J. D.; de Foy, B.; Acevedo Rosas, F.; Caetano, E.; Carmichael, G.; Emmons, L.; McKenna, D.; Mena, M.; Skamarock, W.; Tie, X.; Coulter, R. L.; Barnard, J. C.; Wiedinmyer, C.; Madronich, S. A meteorological overview of the MILAGRO field campaigns. *Atmos. Chem. Phys.* **2007**, *7*, 2233−2257.

(36) Carreón-Sierra, S.; Salcido, A.; Castro, T.; Celada-Murillo, A.-T. Cluster Analysis of the Wind Events and Seasonal Wind Circulation Patterns in the Mexico City Region. *Atmosphere* **2015**, *6*, 1006−1031.

(37) Sistema de Monitoreo Atmosférico. Ciudad de México. http://www.aire.cdmx.gob.mx/default.php?opc=%27aKBhnmI=%27&opcion=Zg (accessed on Wed, December 02, 2020).

(38) Holben, B. N.; Eck, T. F.; Slutsker, I.; Tanré, D.; Buis, J. P.; Setzer, A.; Vermote, E.; Reagan, J. A.; Kaufman, Y. J.; Nakajima, T.; Lavenu, F.; Jankowiak, I.; Smirnov, A. AERONET—A Federated Instrument Network and Data Archive for Aerosol Characterization. *Remote Sens. Environ.* **1998**, *66*, 1−16.

(39) Carabali, G.; Estévez, H. R.; Valdés-Barrón, M.; Bonifaz-Alfonzo, R.; Riveros-Rosas, D.; Velasco-Herrera, V. M.; Vázquez-Gálvez, F. A. Aerosol climatology over the Mexico City basin: Characterization of optical properties. *Atmos. Res.* **2017**, *194*, 190−201.

(40) NASA EOS/Aura Validation Data Center (AVDC)—Correlative data. Field of View Predictions, Data Subsets, GEOMS, DCIO. https://avdc.gsfc.nasa.gov/pub/most_popular/overpass/OMI/ (accessed on 2021-06-16).

(41) Tanskanen, A.; Krotkov, N. A.; Herman, J. R.; Arola, A. Surface ultraviolet irradiance from OMI. *IEEE Trans. Geosci. Rem. Sens.* **2006**, *44*, 1267−1271.

(42) Veefkind, J. P.; de Haan, J. F.; Kroon, M.; Levelt, P. F.; Levelt, P. F. Total Ozone From the Ozone Monitoring Instrument (OMI) Using the DOAS Technique. *IEEE Trans. Geosci. Rem. Sens.* **2006**, *44*, 1239−1244.

(43) Tanskanen, A.; Lindfors, A.; Määttä, A.; Krotkov, N.; Herman, J.; Kaurola, J.; Koskela, T.; Lakkala, K.; Fioletov, V.; Bernhard, G.; McKenzie, R.; Kondo, Y.; O'Neill, M.; Slaper, H.; den Outer, P.; Bais, A. F.; Tamminen, J. Validation of daily erythemal doses from Ozone Monitoring Instrument with ground-based UV measurement data. *J. Geophys. Res.: Atmos.* **2007**, *112*, D24S44.

(44) Arola, A.; Kazadzis, S.; Lindfors, A.; Krotkov, N.; Kujanpää, J.; Tamminen, J.; Bais, A.; di Sarra, A.; Villaplana, J. M.; Brogniez, C.; Siani, A. M.; Janouch, M.; Weihs, P.; Webb, A.; Koskela, T.; Kouremeti, N.; Meloni, D.; Buchard, V.; Auriol, F.; Ialongo, I.; Staneck, M.; Simic, S.; Smedley, A.; Kinne, S. A new approach to correct for absorbing aerosols in OMI UV. *Geophys. Res. Lett.* **2009**, *36*, L22805.

(45) Madronich, S. Intercomparison of NO2 photodissociation and U.V. Radiometer Measurements. *Atmos. Environ.* **1987**, *21*, 569−578.

(46) Shaw, W. J.; Pekour, M. S.; Coulter, R. L.; Martin, T. J.; Walters, J. T. The daytime mixing layer observed by radiosonde profiler, and lidar during MILAGRO. *Atmos. Chem. Phys. Discuss.* **2007**, *7*, 15025−15065.

(47) Velasco, E.; Márquez, C.; Bueno, E.; Bernabé, R. M.; Sánchez, A.; Fentanes, O.; Wöhrnschimmel, H.; Cárdenas, B.; Kamilla, A.; Wakamatsu, S.; Molina, L. T. Vertical distribution of ozone and VOCs in the low boundary layer of Mexico City. *Atmos. Chem. Phys.* **2008**, *8*, 3061−3079.

(48) Greenberg, J. P.; Guenther, A. B.; Turnipseed, A. Tethered balloon-based soundings of ozone aerosols, and solar radiation near Mexico City during MIRAGE-MEX. *Atmos. Environ.* **2009**, *43*, 2672−2677.

(49) Rogers, R. R.; Hair, J. W.; Hostetler, C. A.; Ferrare, R. A.; Obland, M. D.; Cook, A. L.; Harper, D. B.; Burton, S. P.; Shinozuka, Y.; McNaughton, C. S.; Clarke, A. D.; Redemann, J.; Russell, P. B.; Livingston, J. M.; Kleinman, L. I. NASA LaRC airborne high spectral resolution lidar aerosol measurements during MILAGRO: observations and validation. *Atmos. Chem. Phys.* **2009**, *9*, 4811−4826.

(50) Lewandowski, P. A.; Eichinger, W. E.; Holder, H.; Prueger, J.; Wang, J.; Kleinman, L. I. Vertical distribution of aerosols in the vicinity of Mexico City during MILAGRO-2006 Campaign. *Atmos. Chem. Phys.* **2010**, *10*, 1017−1030.

(51) Corr, C. A.; Krotkov, N.; Madronich, S.; Slusser, J. R.; Holben, B.; Gao, W.; Flynn, J.; Lefer, B.; Kreidenweis, S. M. Retrieval of aerosol single scattering albedo at ultraviolet wavelengths at the T1 site during MILAGRO. *Atmos. Chem. Phys.* **2009**, *9*, 5813−5827.

(52) Castro, T.; Madronich, S.; Rivale, S.; Muhlia, A.; Mar, B. The influence of aerosols on photochemical smog in Mexico City. *Atmos. Environ.* **2001**, *35*, 1765−1772.

(53) SEDEMA. *Calidad del aire en la Ciudad de México, Informe 2017*, 2018.

(54) Retama, A.; Baumgardner, D.; Raga, G. B.; McMeeking, G. R.; Walker, J. W. Seasonal and diurnal trends in black carbon properties and co-pollutants in Mexico City. *Atmos. Chem. Phys.* **2015**, *15*, 9693−9709.

(55) Cabrera, S.; Ipiña, A.; Damiani, A.; Cordero, R. R.; Piacentini, R. D. UV index values and trends in Santiago, Chile (33.5°S) based on ground and satellite data. *J. Photochem. Photobiol., B* **2012**, *115*, 73−84.

(56) Zhang, H.; Wang, J.; Castro García, L.; Zeng, J.; Dennhardt, C.; Liu, Y.; Krotkov, N. A. Surface erythemal UV irradiance in the continental United States derived from ground-based and OMI observations: quality assessment trend analysis and sampling issues. *Atmos. Chem. Phys.* **2019**, *19*, 2165−2181.

(57) Vitt, R.; Laschewski, G.; Bais, A.; Diémoz, H.; Fountoulakis, I.; Siani, A.-M.; Matzarakis, A. UV-Index Climatology for Europe Based on Satellite Data. *Atmosphere* **2020**, *11*, 727.

(58) Janjai, S.; Wisitsirikun, S.; Buntoung, S.; Pattarapanitchai, S.; Wattan, R.; Masiri, I.; Bhattarai, B. K. Comparison of UV index from

Ozone Monitoring Instrument (OMI) with multi-channel filter radiometers at four sites in the tropics: effects of aerosols and clouds. *Int. J. Bioclimatol.* **2013**, *34*, 453−461.

(59) Parrish, D. D.; Singh, H. B.; Molina, L.; Madronich, S. Air quality progress in North American megacities: A review. *Atmos. Environ.* **2011**, *45*, 7015−7025.

(60) Secretaría del Medio Ambiente de la Ciudad de México. *Calidad del aire en la Ciudad de México, informe 2017*, 2018; pp 1−160.

(61) Molina, L. T.; Velasco, E.; Retama, A.; Zavala, M. Experience from Integrated Air Quality Management in the Mexico City Metropolitan Area and Singapore. *Atmosphere* **2019**, *10*, 512.

(62) Laskin, A.; Laskin, J.; Nizkorodov, S. A. Chemistry of Atmospheric Brown Carbon. *Chem. Rev.* **2015**, *115*, 4335−4382.

(63) Gadhavi, H.; Jayaraman, A. Absorbing aerosols: contribution of biomass burning and implications for radiative forcing. *Ann. Geophys.* **2010**, *28*, 103−111.

(64) Rios, B.; Raga, G. B. Smoke emissions from agricultural fires in Mexico and Central America. *J. Appl. Remote Sens.* **2019**, *13*, 1.

(65) Barnard, J. C.; Volkamer, R.; Kassianov, E. I. Estimation of the mass absorption cross section of the organic carbon component of aerosols in the Mexico City Metropolitan Area. *Atmos. Chem. Phys.* **2008**, *8*, 6665−6679.